CHEMICAL ENGINEERING TRANSACTIONS
VOL. 43, 2015
A publication of AIDIC
The Italian Association of Chemical Engineering
Online at www.aidic.it/cet
Chief Editors: Sauro Pierucci, Jiří J. Klemeš

ISBN 978-88-95608-34-1; **ISSN** 2283-9216
DOI: 10.3303/CET1543153

Fuel Cell Platinum Catalysts Supported on Mediate Surface Area Carbon Black Supports

Luděk Kaluža[a], Mikkel J. Larsen[b], Miroslav Zdražil[a], Daniela Gulková*[a], Madeleine Odgaard[b]

[a]Institute of Chemical Process Fundamentals of the ASCR, v. v. i.; Rozvojová 135; 165 02 Prague 6 – Suchdol; Czech Republic
[b]IRD Fuel Cells A/S; Kullinggade 31; 5700 Svendborg; Denmark
gulkova@icpf.cas.cz

Five carbon black supports with medium surface area about 400 $m^2\ g^{-1}$ were studied for deposition of 60 wt. % platinum from aqueous solutions of hexachloroplatinic acid by impregnation. The catalysts were compared in terms of X-ray diffraction, Laser Raman spectroscopy, pulse H_2 chemisorption, electrocatalytic properties and electrochemical accelerated stress testing. The deposited Pt exhibited crystallite sizes of about 3.6–8.0 by H_2 chemisorption. The calcination of the dried catalysts prior to their reduction led to higher interaction of the hexachloroplatinic acid with the supports, which resulted in greater electrochemical stability. Dechlorination of the reduced catalysts was performed to decrease the residual content of chlorine species, which resulted in a 1.1–1.7-fold increase in the Pt crystallite size but did not alter the surface area or the electrochemical performance significantly. All of the prepared catalysts exhibited similar electrochemically active surface area, about 30 $m^2\ g_{Pt}^{-1}$, and all showed higher specific electrocatalytic activities toward the oxygen-reduction reaction than that of the commercial high-surface-area reference catalyst, while their mass-specific activities were slightly lower. All five catalysts showed better electrochemical stability of the support than the reference, while the stability of the Pt particles was better for one of them, catalyst Pt/CB3.

1. Introduction

Hydrogen and fuel cells represents a possible solution to meet the environmental restrictions increasingly imposed on transportation (Mert et al., 2010). Carbon-supported platinum represents conventional catalyst in polymer electrolyte membrane full cells (PEMFC). Most catalysts studied in the literature consist of 10-40 wt. % Pt and a Vulcan XC72 (Cabot Corp.) carbon black (CB) as support with specific surface area (S_{BET}) of about 230 $m^2\ g^{-1}$ (Bagotsky, 2012). However, higher loading of Pt is desirable to avoid too thick catalytic layer in the membrane-electrode assembly (MEA) of the PEMFC. Deposition of higher loadings of Pt (about 60 wt. %) in highly dispersed forms remains challenging, though (Fang et al., 2009).
The purpose of the present work was to deposit 60 wt. % of Pt on five different experimental CB supports with S_{BET} of about 400 $m^2\ g^{-1}$. Aqueous solution of hexachloroplatinic acid (H_2PtCl_6) was used for impregnation of the supports. The residual content of Cl was carefully monitored in the prepared catalysts because Cl is a poison to Pt catalysts, it increases the propensity of PEMFC to corrosion and it decreases the catalytic activity in PEMFC (Job et al., 2013). The content of residual Cl in the catalysts was determined by means of determination of hydrolyzable chlorides using ion liquid chromatography (ILC) and of total chlorine using instrumental neutron activation analysis (INAA). The prepared catalysts were compared with a commercial reference catalyst as for structural properties, composition and electrochemical performance.

2. Experimental

2.1 Catalysts preparation

Platinum was deposited onto 5 experimental carbons (IMERYS Graphite & Carbon Ltd., obtained by different production processes and post treatments of standard carbons), labeled CB1 (S_{BET} = 384 $m^2\ g^{-1}$), CB2 (S_{BET} =

Please cite this article as: Kaluza L., Larsen M., Zdrazil M., Gulkova D., Odgaard M., 2015, Fuel cell platinum catalysts supported on mediate surface area carbon black supports, Chemical Engineering Transactions, 43, 913-918 DOI: 10.3303/CET1543153

385 m^2 g^{-1}), CB3 (S_{BET} = 452 m^2 g^{-1}), CB4 (S_{BET} = 371 m^2 g^{-1}) and CB5 (S_{BET} = 379 m^2 g^{-1}) to prepare catalysts with nominal loading of Pt = 60 wt. %. Solution of H_2PtCl_6 (250 g_{Pt} L^{-1}, Safina, lot no. VMC00269/011013) was diluted with 10 mL of distilled water in a round distillation flask, and 2 g of carbon was immersed into the solution. The mixture was heated under reflux condenser at 80 °C for 2 h. The sample was allowed to cool to laboratory temperature an then it was dried in a rotary vacuum evaporator at 95 °C for 4 h. The samples were calcined in Ar at 190 °C for 1 h with a temperature ramp of 5 °C min^{-1} and reduced in a mixture of H_2 (5 %) and Ar at 190 °C for 1 h with a temperature ramp of 5 °C min^{-1}. The catalysts were poured under Ar to glass ampules and labeled as Pt(Cl)/CB1, Pt(Cl)/CB2, Pt(Cl)/CB3, Pt(Cl)/CB4, Pt(Cl)/CB5. Part of the dried sample with CB1 was not calcined but it was only reduced as described above. It was labeled as Pt(Cl,R)/CB1. 1 g of each catalyst was then dechlorinated by 0.1 M solution of sodium hydroxide in distilled water. The sample was dispersed by vibration for 30 min and then centrifuged for about 10 min with 2500–4000 revolutions per minute (rpm) at room temperature. The separated solution was analyzed for Cl^- content by ILC with a Dionex ICS-5000 instrument equipped with an AS11-HC column (Thermo Scientific Inc., 2 x 250 mm, product no. 052961). Then, distilled water was added and the centrifugation-extraction process was continued until the test on Cl^- content was negative and the pH of the solution was about 6. The washed catalysts were dried in a desiccator overnight and then re-reduced (the same conditions as above). These dechlorinated final catalysts were labeled as Pt/CB1, Pt/CB2, Pt/CB3, Pt/CB4, and Pt/CB5. The actual content of Pt in the final catalysts was determined by SEM-EDX, which confirmed 60 ± 2 wt. %. The content of residual total chlorine in the catalysts was determined by INAA using a reference material, NIST SRM 1547 (Peach Leaves), for quantification of the chlorine content (U.S. National Institute of Standards and Technology, 1993). The content of hydrolyzable chlorides was determined in the liquid after extraction as described above.

2.2 Microstructural characterization

X-ray diffraction (XRD) patterns were recorded on a Bruker D8 Discover diffractometer equipped with LynxEye detector using Cu K-alpha radiation (40 kV, 40 mA) and a graphite monochromator. The rate of measurements was 0.013 ° per 1.5 s. The patterns were processed with the program FullProf and the LeBail fitting method (Rodríguez-Carvajal, 2001). The size of Pt crystallites ($d_{Pt,XRD}$) was calculated by the use of the Scherrer equation and the reflection angles 39.8, 46.3, 67.5, 81.3, 85.8 °. Laser Raman spectra (LRS) were collected using a dispersive Nicolet Almega XR spectrometer equipped with an Olympus BX51 microscope and an excitation laser source (473 nm), and with an incident power of 5 mW with 256 expositions with 0.5 s exposition time. The size of turbostratic graphite crystallites ($d_{G,LRS}$) were approximated from the D and G band intensity ratio as it was published elsewhere (Tuinstra and Koenig, 1970) (details in Results and discussion). N_2 adsorption isotherms were measured using a Micromeritics ASAP 2010M instrument. Before these measurements, the samples were evacuated at 120 °C for 12 h. S_{BET} was determined by the Brunauer–Emmett–Teller (BET) procedure. H_2 pulse chemisorption was measured using a Micromeritics chemisorber AutoChem 2950 HP at -60 °C. The surface area of the metallic platinum ($S_{Pt,H2}$) was calculated form the amount of chemisorbed H_2 assuming that the Pt:H chemisorption stoichiometry was 1:1 and that the number of surface atoms per unit area was 1.25 10^{19} at. m^{-2} as it was reported elsewhere (Anderson and Pratt, 1985). The theoretical diameter of the platinum crystallites ($d_{Pt,H2}$) was calculated assuming spherical geometry and uniform particle size.

2.3 Electrochemical characterization

The performance of the catalysts was evaluated by cyclic voltammetry (CV) using a rotating-disc electrode (RDE) approach. Suspensions of catalyst, water, alcohol and ionomer were made, from which electrodes with a loading of 183 μg_{Pt} cm^{-2} were prepared on a Pine AFE3T050GC glassy-carbon RDE disc by a drop-coating procedure. All measurements were done in 34 ± 3 °C, 0.10 M aqueous $HClO_4$ electrolyte in a glass cell equipped with a Pt-wire counter electrode in a glass-fritted glass tube and a Radiometer Analytical REF621 mercury–mercurous-sulfate (MMS) reference electrode with a potential of 0.72 V vs. the reversible hydrogen electrode (RHE). A Pine AFMSRCE rotator and a Bio-Logic SP-150 potentiostat were used, and control and data acquisition was done via EC-Lab v. 10.32 software. All potentials stated here refer to RHE.

The electrochemically active surface area (*ESA*) of the platinum was determined from voltammograms recorded in N_2-saturated electrolyte. 15 or more cyclic voltammograms between 0.05 V and 1.10 V vs. RHE were recorded at a scan rate of 20 mV s^{-1}. The resulting hydrogen-desorption charge was determined by integration of the positive peak in a region from about 0.06 to about 0.4 V vs. RHE of the last of the recorded N_2 CVs, using a horizontal baseline. The *ESA* was obtained by division by 0.21 mC cm^{-2}.

The electrocatalytic activity toward the oxygen-reduction reaction (ORR) was evaluated from voltammograms recorded in O_2-saturated electrolyte. 15 or more CVs between 0.05 V and 1.10 V vs. RHE were recorded at a scan rate of 20 mV s^{-1} and rotation speed of 1,600 rpm. The potential chosen for the evaluation of ORR

activity was 0.90 V vs. RHE. The current at this potential ($I_{0.90\ V}$), was evaluated as the average of the current values for the positive-going and negative-going sweeps of the last of the recorded O_2 CVs. A Koutecky–Levich approach was applied in order to extract the kinetic current (I_k) from the measured (total) current. This I_k was then normalized to the *ESA* of the sample to give the specific activity (i_k) and to the mass of Pt in the electrode (m_{Pt}) to give the mass-specific activity ($i_{k,mass}$) by $i_k = -I_k/ESA$ and $i_{k,mass} = -I_k/m_{Pt}$, respectively.
After the initial recording of CVs for *ESA* and ORR-activity determinations, respectively, the electrode was subjected to one of three different electrochemical accelerated stress test (AST) procedures: a) 3,000 CVs between 0.60 V and 1.20 V vs. RHE at 200 mV s^{-1} in O_2-saturated electrolyte (overall oxidative ageing, 5 h total time); b) 30,000 square-wave cycles (SWCs) between 0.60 V and 0.95 V vs. RHE, 3 s hold time at each potential limit, in N_2-saturated electrolyte (mainly ageing of the Pt catalyst, 53 h total time including characterization); and c) 60,000 CVs between 1.0 V and 1.5 V vs. RHE at 500 mV s^{-1} in N_2-saturated electrolyte (mainly ageing of the carbon support, 38 h total time including characterization) (Ohma et al., 2011). No rotation was applied during the AST procedures (apart from brief regular sequences in procedures b) and c) for the removal of possible gas bubbles from the electrode). The intermediate characterization in b) and c) involved the recording of 10 CVs between 0.05 V and 0.60 V vs. RHE for *ESA* determination after each 5,000 AST cycles (and more frequently in the initial stages of the procedures). Recording of CVs for ORR-activity determination (including Koutecky–Levich analysis) and *ESA* determinations was repeated after ageing was completed.

3. Results and discussion

3.1 Concept of catalyst preparation

The preparation procedure was mainly followed by H_2 chemisorption (Table 1). It was found that the reduced Pt species (catalyst Pt(Cl,R)/CB1) exhibited a high $S_{Pt,H2}$ of 74 $m^2\ g_{Pt}^{-1}$. Calcination in Ar at 190 °C prior to the reduction (catalyst Pt(Cl)/CB1) led to about 31 % decrease of $S_{Pt,H2}$. The calcination, however, appeared to play a crucial role for increasing the stability towards electrochemical ageing as it is shown below in section 3.3 (*ESA* decrease of 24 % vs 54 % during oxidative AST, cf. Table 2). All catalysts were therefore calcined before the reduction. High interaction of the deposited H_2PtCl_6 species with the carbon support during the calcination could explain this observation.
The values of hydrolyzable chlorides and total chlorine are summarized in Table 1. The highly dispersed Pt catalyst, Pt(Cl,R)/CB1, which was prepared by direct reduction of deposited H_2PtCl_6 in H_2 without pre-calcination, exhibited an about 8-fold higher value of hydrolyzable Cl^- and an about 1.7-fold higher value of total Cl than the studied commercial reference catalyst, HiSPEC® 9100 (Ref. Pt/C). The prepared catalysts were therefore dechlorinated. The dechlorination procedure was found to decrease the values of hydrolyzable Cl^- to about the same level as it was found for Ref. Pt/C. The amount of total Cl in the final prepared catalysts remained relatively high, but about the same as in Ref. Pt/C. Ref. Pt/C exhibited a more than 10-fold higher value of total Br than it was observed for the prepared catalysts. It is believed that only the Pt precursor such as H_2PtCl_6 is responsible for chlorination (or bromination) of the catalysts because the original carbon, CB1 for example, contained only about 10 ppm of total Cl and Br.

Table 1: Catalysts properties

Catalysts	H_2 uptake mmol g^{-1}	$S_{Pt,H2}$ $m^2\ g_{Pt}^{-1}$	$d_{Pt,H2}$ nm	$d_{Pt,XRD}$ nm	Hydrolyzable Cl^-, ppm	Total Cl, ppm	Total Br, ppm	S_{BET} $m^2\ g^{-1}$
Pt(Cl,R)/CB1	462	74	3.8	-	600	2,530	<10	135
Pt(Cl)/CB1	317	51	5.6	-	-	-	-	142
Pt(Cl)/CB2	292	47	6.1	-	-	-	-	141
Pt(Cl)/CB3	491	79	3.6	-	-	-	-	184
Pt(Cl)/CB4	307	49	5.8	-	-	-	-	133
Pt(Cl)/CB5	272	44	6.5	-	-	-	-	140
Dechlorinated catalysts:								
Pt/CB1	223	36	8.0	10.0	70	1,530	<10	141
Pt/CB2	261	42	6.8	11.4	70	1,460	<10	149
Pt/CB3	293	47	6.1	11.4	70	1,380	<10	193
Pt/CB4	264	42	6.7	13.4	70	1,950	<10	136
Pt/CB5	220	35	8.0	11.4	70	2,030	<10	143
Reference catalyst:								
Ref. Pt/C	456	77	3.7	3.2[A]	<74[A]	1,480	131	359

[A] Provided by the manufacturer

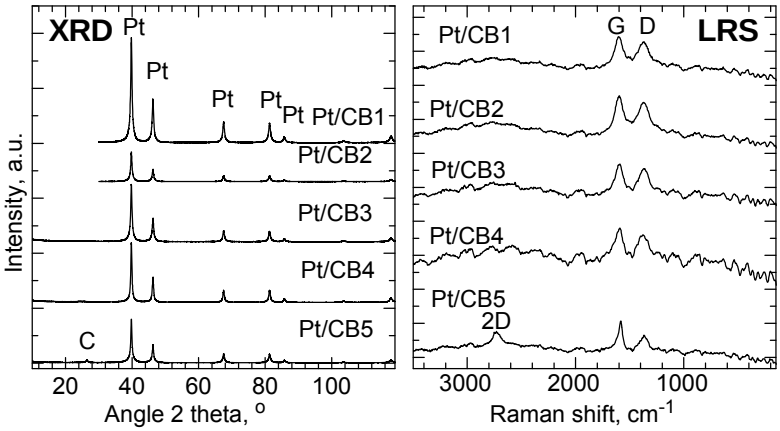

Figure 1: Structural analysis of the studied catalysts by XRD: Pt – cubic platinum; C – graphitic carbon; and by LRS: G band - graphitic carbon; D and 2D bands – disordered carbon

Whereas the applied dechlorination procedure is found to decrease the values of hydrolyzable Cl^- and of total Cl to acceptable levels, it also caused further decrease (by 11–42 %) of $S_{Pt,H2}$ for all catalysts; e.g., by about 29 % from 51 $m^2\ g_{Pt}^{-1}$ to 36 $m^2\ g_{Pt}^{-1}$ for Pt/CB1 (Table 1).

3.2 Microstructural properties of the catalysts

Structural analyses of the prepared catalysts were done by XRD and LRS. The XRD patterns (Figure 1) clearly reveal the presence of highly isomorphic Pt crystallites of cubic structure. The values of $d_{Pt,XRD}$ are somewhat higher than those of $d_{Pt,H2}$ (Table 1). A plausible explanation for this is that pulse chemisorption of H_2 is sensitive to all Pt species amplifying the atomically dispersed species, while XRD reflects only on the crystalline Pt amplifying the largest crystals. Nevertheless, irrespective of the determination method, the Pt-particle diameters for the prepared catalysts were higher than the values reported for the industrial reference catalyst.

LRS showed that the catalysts Pt/CB1-Pt/CB4 exhibited practically the same patterns with low-intensity bands D and G at 1,375 and 1,580 cm^{-1}, respectively (Figure 1). The intensity ratio of the D band to the G band (I_D/I_G) was approximately 1. Correlation between I_D/I_G and graphitic particle size (Tuinstra and Koenig, 1970) shows that this corresponds to a size of graphitic crystallites $d_{G,LRS}$ of about 5 nm. Because the full width at half maximum intensity of the G band was larger than 20 cm^{-1} for all supports, the degree of graphitization was low, and the graphitic crystallites have highly turbostratic character (Yoshida et al., 2006). Nevertheless, the patterns of Pt/CB5 differed slightly: I_D/I_G was approximately 0.7, which corresponds to a $d_{G,LRS}$ about 6.7 nm. Qualitatively this correlated well with the XRD pattern of Pt/CB5, in which a somewhat pronounced peak at 2 theta = 26.5 ° was also identified, which is ascribed to graphitic crystallinity. From this peak a rather tentative value of the graphitic crystallite size $d_{G,XRD}$ of about 17 nm can be calculated by the Scherrer equation. Interestingly, a 2D band was additionally found in the laser Raman spectrum of Pt/CB5 at about 2,700 cm^{-1}, which is significant of disordered carbon. It was concluded that Pt/CB5 contained larger graphitic crystallites but also had higher content of amorphous carbon than the other prepared catalysts.

The S_{BET} of the prepared catalysts was analyzed by N_2 physisorption and is listed in Table 1. As for the raw support materials, CB3 with 452 $m^2\ g^{-1}$ exhibited more than 15 % higher S_{BET} than the other four experimental supports (survey in Experimental), which exhibited about the same S_{BET}. The deposition of the Pt in the final catalysts resulted in practically proportionate decrease of S_{BET}. Thus the catalyst Pt/CB3 kept the highest S_{BET} (193 $m^2\ g^{-1}$) among the studied catalysts.

Sample Pt/CB3 also showed the smallest $d_{Pt,H2}$ among the final dechlorinated catalysts, namely 6.1 nm. The Pt on the other four catalysts seems to be slightly less dispersed, with values of $d_{Pt,H2}$ of 6.7–8.0 nm. The dispersion may to some extent be linked to the S_{BET} of the applied supports, but probably more importantly to various surface and pore structural properties of these. The lowest Pt dispersion is observed for Pt/CB5 ($S_{Pt,H2}$ = 35 $m^2\ g_{Pt}^{-1}$, $d_{Pt,H2}$ = 8.0 nm), but this is not significantly lower than that of the other catalysts. Thus good dispersion is achieved even for this catalyst with large graphitic domains.

3.3 Electrochemical characteristics

The values of relevant electrochemical parameters extracted from the cyclic voltammograms are shown in Table 2. All experimental samples show specific *ESA*s around 30 $m^2\ g_{Pt}^{-1}$. However, the *ESA*s of the samples Pt/CB4 and Pt/CB5 are slightly lower than those of the samples Pt/CB1, Pt/CB2 and Pt/CB3. Sample Pt/CB3

shows the highest *ESA* of 32 m^2 g_{Pt}^{-1}, which is in good accordance with the fact that the highest $S_{Pt,H2}$ was found for this sample (Table 1). For Pt/CB3 the ratio between *ESA* and $S_{Pt,H2}$ is 0.69, meaning that 69 % of the total Pt surface area is available for electrochemical reaction in the electrode prepared for the RDE measurements. Generally for the five dechlorinated catalysts this proportion is 64–85 %. For the five non-dechlorinated catalysts it is only 45–65 %, indicating that the purification and rearrangement taking place during the dechlorination procedure are beneficial in terms of electrochemical utilization of the Pt, either by creating a surface that is better suited for electroadsorption or by improving the electrical contact between the Pt phase and the support, or both.

In terms of mass-specific ORR activity Pt/CB1, Pt/CB2 and Pt/CB3 (and their corresponding non-dechlorinated versions) perform best, all showing around 30 A g_{Pt}^{-1}. This is around 25 % lower than the high-surface-area reference catalyst. On the other hand, the specific activity for the three best catalysts is around 100 µA cm^{-2}, which is nearly twice as high as that of Ref. Pt/C. This is likely due the phenomenon called the particle size effect: the surface of larger Pt nanoparticles is more active due to increased prevalence of the most active crystal facet (Kinoshita, 1992). The least active catalyst samples are those based on CB4 and CB5. Especially CB5 (i.e., the one with the large graphitic domains) seems to result in catalysts that perform poorly in terms of activities. This observation could be associated with less beneficial interactions between the Pt phase and this support compared to the other supports. Also, it could arise from difficulties in obtaining a good electrode structure with this catalyst due to the clearly different nature of its support material.

As for the stability, it is observed that all three applied ASTs cause considerable degradation of the *ESA* of the catalysts. Among the dechlorinated catalysts, Pt/CB4 and Pt/CB5 have the highest degradation levels. The oxidative AST (which is designed to give dissolution of the Pt particles as well as corrosion of the carbon support) results in higher *ESA* degradation for these two catalysts than for Ref. Pt/C, while it is somewhat lower than this for Pt/CB1, Pt/CB2 and Pt/CB3. However, the *ESA* degradation during support-focused AST (designed for inducing primarily carbon corrosion) is significantly smaller for all five catalysts than for Ref. Pt/C, which shows the benefit of using a CB support with moderate surface area instead of a high-surface-area CB support. During the catalyst-focused AST (designed for inducing primarily Pt dissolution) Pt/CB1, Pt/CB2 and Pt/CB5 show about the same *ESA* degradation as Ref. Pt/C, while that for Pt/CB4 is higher and that for Pt/CB3 lower. The catalyst Pt/CB3 with the smallest particles and largest *ESA* among the five dechlorinated catalysts thus appears to have the best catalyst stability; however, its support stability is the lowest among the five, though it is still higher than that of the reference.

As mentioned earlier, calcination seems to greatly increase the electrochemical stability in terms of *ESA* (Pt(Cl,R)/CB1 vs. Pt(Cl)/CB1, Table 2). As for dechlorination, its effect on the *ESA* stability is rather ambiguous: almost negligible for Pt/CB1 and Pt/CB5, increasing for Pt/CB2 and Pt/CB3, and decreasing for Pt/CB4. However, the major positive effect of the dechlorination (poison removal) is expected to be observed during fuel-cell operation with MEAs rather than in RDE experiments, which are carried out in a large quantum of liquid electrolyte capable of diluting any chlorides released from the catalyst.

The specific activity changes either negatively or positively during the ASTs, which is to be qualitatively explained by the mechanisms taking place during the individual AST procedures. The catalyst-focused AST is

Table 2: Electrochemical properties

Catalysts	*ESA*	Change in *ESA* during ageing			ORR activity at 0.90 V		Change in i_k during ageing		
		Oxidative	Catalyst	Support	$i_{k,mass}$	i_k	Oxidative	Catalyst	Support
	m^2 g_{Pt}^{-1}	%	%	%	A g_{Pt}^{-1}	µA cm^{-2}	%	%	%
Pt(Cl,R)/CB1	34	-54	-	-	33	96	37	-	-
Pt(Cl)/CB1	32	-24	-66[A]	-38[A]	34	105	0	-18[A]	62[A]
Pt(Cl)/CB2	30	-37	-	-	31	103	14	-	-
Pt(Cl)/CB3	35	-42	-	-	34	97	3	-	-
Pt(Cl)/CB4	32	-35	-	-	24	75	2	-	-
Pt(Cl)/CB5	27	-41	-	-	17	61	12	-	-
Dechlorinated catalysts:									
Pt/CB1	30	-21	-69[B]	-34[B]	29	94	-2	-41[B]	21[B]
Pt/CB2	30	-25	-68	-33	31	102	4	-23	40
Pt/CB3	32	-29	-58	-46	31	94	-10	-1	16
Pt/CB4	27	-47	-78	-36	24	101	31	-28	48
Pt/CB5	26	-37	-66	-39	15	59	9	-14	13
Reference catalyst:									
Ref. Pt/C	76	-35	-66	-53	41	54	22	20	62

[A] Measured for a different, but similarly prepared sample; [B] Averages for two similarly prepared samples

seen to result in a decrease in specific activity for all the novel samples. During this procedure Pt will dissolve, whereby the catalyst nanoparticles will shrink and thus become less active due to the before-mentioned particle-size effect. For the support-focused AST, on the other hand, the specific activity increases for all samples. Under the applied conditions the Pt surfaces are passivated, which prevents dissolution, while the carbon corrodes, which leads to a loss of anchoring points for the Pt particles on the carbon surface. The mobility of the Pt particles is thus increased, and those remaining on the surface can merge into larger particles, which are more active as inferred from the particle-size effect. During the overall oxidative AST, both processes (and many more) can occur, and thus the specific activity can increase or decrease depending on which process is dominant.
Generally, assessment of the suitability of the catalysts based on the AST data depends on what application the PEMFC is intended for; i.e., the ageing conditions that will prevail during its use.

4. Conclusion

Catalysts were successfully prepared from the five different carbon blacks by impregnation with hexachloroplatinic acid, calcination, reduction and dechlorination. Calcination was found to greatly increase the electrochemical stability. Dechlorination resulted in a 1.1–1.7-fold increase of the Pt crystallites, but did not alter the S_{BET}. Furthermore, the *ESA* did not change significantly upon dechlorination, indicating that the purification and rearrangement taking place during the dechlorination procedure are beneficial in terms of electrochemical utilization of the Pt. The prepared catalysts exhibited similar *ESA* of about 30 $m^2\ g_{Pt}^{-1}$, and all showed higher specific electrocatalytic activities toward the ORR than that of the commercial high-surface-area reference catalyst of S_{BET} = 359 $m^2\ g^{-1}$, while their mass-specific ORR activities were slightly lower. All five catalysts showed better electrochemical stability of the support than the reference, which shows the benefit of using a support with moderate surface area. The stability of the Pt particles was better than the reference for one of the catalysts, namely Pt/CB3. This catalyst also had the highest S_{BET} (193 $m^2\ g^{-1}$), the smallest Pt particles (6.1 nm), the best mass-specific ORR activity (31 A g_{Pt}^{-1}) and the lowest residual Cl content (1380 ppm). It could be concluded that the high S_{BET} of CB3 within the moderate-surface-area CB supports is by far the most critical parameter influencing *ESA* and electrochemical stability. Catalyst manufacture based on the carbon type with large graphitic domains (CB5) was found to result in catalysts that perform poorly in terms of activities.

Acknowledgements
IMERYS Graphite & Carbon Ltd. (Switzerland) is kindly acknowledged for the preparation of experimental carbons. The research leading to these results has received funding from the EU's 7th Framework Programme through the Fuel Cells and Hydrogen Joint Technology Initiative under Grant Agreement No. 303466 and project acronym IMMEDIATE. L.K., M.Z. and D.G. highly acknowledge the co-financing of the Ministry of Education, Youth and Sports of the Czech Republic (grant no. 7HX13003).

References

Anderson J.R., Pratt K.C., 1985, Introduction to characterization and testing of catalysts. Academic Press, North Ryde, Australia.
Bagotsky V.S., 2012, Fuel Cells, Problems and Solutions. Wiley, Hoboken, USA.
Fang B., Chaudhari N.K., Kim M.S., Kim J.H., Yu J.S., 2009, Homogeneous deposition of platinum nanoparticles on carbon black for proton exchange membrane fuel cell. J. Am. Chem. Soc., 131, 15330–15338.
Job N., Chatenet M., Berthon-Fabry S., Hermans S., Maillard F., 2013, Efficient Pt/carbon electrocatalysts for proton exchange membrane fuel cells: avoid chloride-based Pt salts!, J. Power Sources, 240, 294–305.
Kinoshita K., 1992, Electrochemical Oxygen Technology. John Wiley & Sons, Inc., New York, USA.
Mert S.Q., Özcelik Z., Özcelik Y., Dincer I., 2010, Multi-objective optimization of a PEM Fuel Cell System, Chemical Engineering Transactions, 21, 877–882.
Ohma A., Shinohara K., Iiyama A., Yoshida T., Daimaru A., 2011, Membrane and Catalyst Performance Targets for Auomotive Fuel Cells by FCCJ Membrane, Catalyst, MEA WG, ECS Trans., 41, 775–784:
Rodríguez-Carvajal J., 2001, Recent developments of the program FullProf. Commission on Powder Diffraction (IUCr) Newsletter, 26, 12–19.
Tuinstra F., Koenig J. L., 1970, Raman spectrum of graphite, J. Chem. Phys., 53, 1126–1130.
U.S. National Institute of Standards and Technology, 1993, Certificate of Analysis, Standard Reference Material 1547, Peach Leaves, Gaithersburg MD20899, USA, January 22, 2013.
Yoshida A., Kaburagi Y., Hishiyama Y., 2006, Full width at half maximum intensity of the G band in the first order Raman spectrum of carbon material as a parameter for graphitization, Carbon, 44, 2333–2335.